PHYSICAL SCIENCES

Nanomotor-enhanced transport of passive Brownian particles in porous media

Anni Shi[1], Haichao Wu[2], Daniel K. Schwartz[1]*

Artificial micro/nanomotors are expected to perform tasks in interface-rich and species-rich environments for biomedical and environmental applications. In these highly confined and interconnected pore spaces, active species may influence the motion of coexisting passive participants in unexpected ways. Using three-dimensional super-resolution single-nanoparticle tracking, we observed enhanced motion of passive nanoparticles due to the presence of dilute well-separated nanomotors in an interconnected pore space. This enhancement acted at distances that are large compared to the sizes of the particles and cavities, in contrast with the insignificant effect on the passive particles with the same dilute concentration of nanomotors in an unconfined liquid. Experiments and simulations suggested an amplification of hydrodynamic coupling between self-propelled and passive nanoparticles in the interconnected confined environment, which enhanced the effective energy for passive particles to escape cavities through small holes. This finding represents an emergent behavior of confined nanomotors and suggests new strategies for the development of antifouling membranes and drug delivery systems.

INTRODUCTION

Self-propulsion and active matter have emerged as intriguing fields of basic research. Beyond biological examples such as bacteria and molecular motors, artificial micro- and nanomotors have drawn extensive attention due to the fundamental interest in their emergent collective behaviors and broad potential applications [e.g., environmental remediation (*1*) and drug delivery (*2*, *3*)]. The study of active particles in bulk and pseudo–two-dimensional (2D) environments is well established (*4*–*9*), and there is growing interest in their behavior in 3D complex interface-rich and species-rich environments, where unexpected phenomena have been observed (*10*–*12*). For example, Bhattacharjee and Datta (*10*) observed trap-and-hop trajectories of bacteria in 3D porous media with barriers in contrast with the expected run-and-tumble behavior. Furthermore, Wu *et al.* (*11*) reported a unique surface-searching transport mechanism of artificial nanomotors in interconnected porous media, where confined nanomotors moved along interior walls and efficiently found exits to translocate to neighboring cavities, in contrast with the prolonged trapping of passive Brownian particles by strong electrostatic repulsion (*13*–*15*). These findings demonstrate the ability of micro/nanomotors to effectively explore their surroundings, suggesting potential applications in crowded, complex, and porous environments.

Many proposed applications of nanomotors, including therapeutic delivery agents (*16*–*18*), catalysts (*19*, *20*), and sorbents (*21*, *22*), involve complex biological, industrial, and geological environments. While less frequently described, active particles can also potentially act as promoters, enhancing the transport and performance of coexisting passive participants. Such uses are particularly attractive because of the possibility that active species could be used in low concentrations to enhance existing technologies. The general concept has precedent. For example, active biological matter often coexists with inactive obstacles, and the mixing of two species can affect both active swimming and passive diffusion (*23*), which has become a core interest in the field. Self-propulsion of artificial active colloids is reported to control self-assembly (*24*, *25*) and directional transport (*26*–*28*) of passive particles based on hydrodynamic interactions (*29*). For example, researchers observed demixing of active-passive mixtures in a confined 2D environment and leveraged this phenomenon to separate two types of colloids into different chambers (*30*).

Notably, such effects generally require crowded systems (*5*, *31*, *32*). This necessitates large concentrations of active particles, which may be inappropriate for many applications. Moreover, for the confined and complex environments relevant to applications like membrane separations and tissue culture, enhanced transport of passive participants would require communication between active and passive particles across interfaces and at distances that are large relative to the characteristic particle sizes. We speculated that such amplified long-range effects might be present in the highly confined and interconnected void space of 3D porous materials, due to the anomalously efficient and rapid translocation of active particles from confined cavities, which may influence passive species separated by interfaces and distance.

To address this question, we used super-resolution single-particle 3D tracking to investigate how a dilute concentration of nanomotors influences the confined transport of passive nanoparticles in a porous medium. Contrary to the insignificant interactions in an unconfined dilute particle solution, we observed a 4× increase in the motility and a 2× enhancement in the cavity escape efficiency of passive particles when nanomotors were present in the porous medium, even at dilute concentrations such that the average particle-particle separation was many cavity diameters and the probability of colocalization in the same cavity was negligible. The quantitative analysis of particle trajectories combined with computational simulations indicated that hydrodynamic effects from nanomotors may enhance the effective energy of passive particles to escape cavities along streamlines by the order of k_BT (where k_B

[1]Department of Chemical and Biological Engineering, University of Colorado Boulder, Boulder, CO 80309, USA. [2]School of Engineering and Applied Sciences, Harvard University, Cambridge, MA, 02138, USA.
*Corresponding author. Email: daniel.schwartz@colorado.edu

is the Boltzmann constant), which can be tuned by fuel concentration and nanomotor density. These findings suggest that hydrodynamic effects from nanomotors are magnified and spatially extended within narrow and interconnected pore spaces, inviting theoretical studies on the impact of active particles in confined environments. Moreover, the improved motility of confined passive species by nanomotors suggests potential applications for active colloids, including new principles for the design of antifouling technologies.

RESULTS

Tracking fluorescent passive particles with 3D imaging

As model porous media, silica inverse opal films were synthesized by evaporative coassembly of sacrificial template polystyrene particles (d = 500 nm) with a hydrolyzed silicate sol-gel precursor solution (see the Supplementary Materials for details) (*33*). Inverse opals comprise a hexagonally close-packed array of spherical cavities with 12 holes connecting each cavity to neighboring cavities, allowing confined tracer particles to explore individual cavity structures and to translocate between adjacent cavities. Tracer particles comprised passive fluorophore-labeled polystyrene nanoparticles (d = 40 nm), mixtures of nonfluorescent passive nanoparticles and active fluorescent Pt-polystyrene Janus particles of the same size, or mixtures of fluorescent passive and nonfluorescent active particles. Unless otherwise specified, passive and active particles with a mixing ratio of 1:5 were dispersed in a refractive index-matched glycerol/water (w/w = 70%) solution with a total concentration ranging from 10^{-16} to 10^{-15} M, ensuring that the particles were well separated in the inverse opal film (fig. S1).

Hydrogen peroxide was introduced into the inverse opal 1 min before the onset of video acquisition, acting as fuel to power Pt-polystyrene Janus nanomotors through self-diffusiophoresis initiated by H_2O_2 decomposition. On the basis of a standard Stokes-Einstein calculation, the diffusion coefficient of the H_2O_2 molecules in the refractive index-matching solution was estimated to be ~50 $\mu m^2/s$, facilitating rapid diffusion into the entire inverse opal film (thickness, 5 to 10 μm). The structure of the inverse opal comprised cavities with a diameter of 530 ± 48 nm, linked by 12 holes with a diameter of 136 ± 10 nm, as detailed in fig. S2, and the approximate time required for H_2O_2 to diffuse a distance corresponding to a cavity diameter was on the order of 10 ms. With additional mixing due to advection from the nanomotors, it is likely that the fuel concentration maintained a relatively uniform distribution in the porous film with only minor spatial variation. Consistent with this, individual nanomotors exhibited consistent motion throughout their trajectories.

To quantitatively study the influence of nanomotors on the cavity-escape process of passive Brownian particles, we performed 3D single-particle tracking and acquired over 70 particle trajectories in order to perform a robust statistical analysis on the fluorescent passive particles in the presence of Janus nanomotors within the interconnected pore space of an inverse opal (Fig. 1A). 3D tracking was achieved by combining variable-angle illumination epifluorescence microscopy with double-helix point spread function imaging using a SPINDLE module (Double Helix Optics Inc.) (Fig. 1B). In this approach, the axial (depth) position is encoded into the shape of the function, specifically the orientation of the high intensity lobes (*34*). 3D trajectories and spatiotemporal coordinates revealed the cavity exploration process of Brownian particles and nanomotors in the inverse opal. Consistent with a previous report (*11*), nanomotors moved along the internal cavity surfaces and escaped from exits efficiently (Fig. 1, C and D). The motion of a given nanomotor did not change measurably over the course of an experiment, either in bulk solution or in inverse opals, suggesting that fuel concentration gradients were much too small to result in substantial local diffusioophoretic effects. Passive particles, on the other hand, typically explored the entire 3D volume of a cavity before escaping to a neighboring cavity (Fig. 1, E and F). In the presence of nanomotors, however, the exploration time of passive particles in a given cavity was significantly reduced (Fig. 1, G and H). This phenomenon qualitatively demonstrated that the presence of nanomotors, even at dilute concentrations, activated (i.e., enhanced) the transport and cavity-escape efficiency of passive particles in a confined environment.

Nanomotor-enhanced transport of passive Brownian particles in confinement

The time evolution of transport was quantitively analyzed using the time- and ensemble-averaged mean squared displacement (MSD), $\langle \Delta \mathbf{r}(\tau)^2 \rangle = \langle |\mathbf{r}(t+\tau) - \mathbf{r}(t)|^2 \rangle$, where t represents elapsed time within a trajectory, τ represents the lag time, $\mathbf{r}$ denotes the 3D position, and <...> represents averaging over all time intervals within all trajectories (Fig. 2A). Diffusion coefficients were calculated by fitting the 3D MSD to the expression MSD = $6D\tau$, over the relevant short- and long-time lag-time ranges. For particles in a bulk glycerol/water solution, the apparent diffusion coefficient of nanomotors (due to rapid rotational diffusion that randomized the direction of the active motion) was 0.63 ± 0.01 $\mu m^2/s$ in the presence of 3% H_2O_2 fuel. The MSD of passive particles grew linearly with τ, as expected for Fickian diffusion, yielding a modestly smaller diffusion coefficient of 0.50 ± 0.01 $\mu m^2/s$. With a small concentration of nanomotors, the diffusion coefficient of passive particles (0.51 ± 0.01 $\mu m^2/s$) was unchanged in solution within experimental error. Thus, in the absence of a confining environment, the presence of a dilute concentration of nanomotors had a negligible impact on the mobility of passive nanoparticles. This was expected because the typical distance between nanomotors and passive particles was much greater than the characteristic particle size.

In an inverse opal with 500-nm-diameter cavities and 136-nm holes (figs. S2 and S3), the motion of all particles was suppressed by confinement effects, e.g., hydrodynamic drag associated with vicinal surfaces (*35*, *36*). Thus, at short lag times ($t \leq 100$ ms), both types of particles exhibited slower but approximate Fickian diffusion associated with intracavity motion (before encountering repulsion from cavity walls). Isolated Brownian particles (in the absence of nanomotors) moved with an apparent short-time diffusion coefficient of $D_{passive}$ = 0.038 ± 0.005 $\mu m^2/s$. The short-time motion of nanomotors, assisted by self-propulsion, was not suppressed as much compared to unconfined motion and exhibited a short-time diffusion coefficient, $D_{nanomotor}$ = 0.082 ± 0.007 $\mu m^2/s$, that was 2.5× higher than that of passive particles. Notably, although unchanged by the presence of nanomotors in bulk (unconfined) liquid, the apparent diffusion of confined activated Brownian particles was enhanced by 47% ($D_{3\%\ activated}$ = 0.055 ± 0.005 $\mu m^2/s$) in the presence of nanomotors. This suggested that long-range hydrodynamic coupling between self-propelled nanomotors and passive particles, while negligible in unconfined liquid, was amplified and

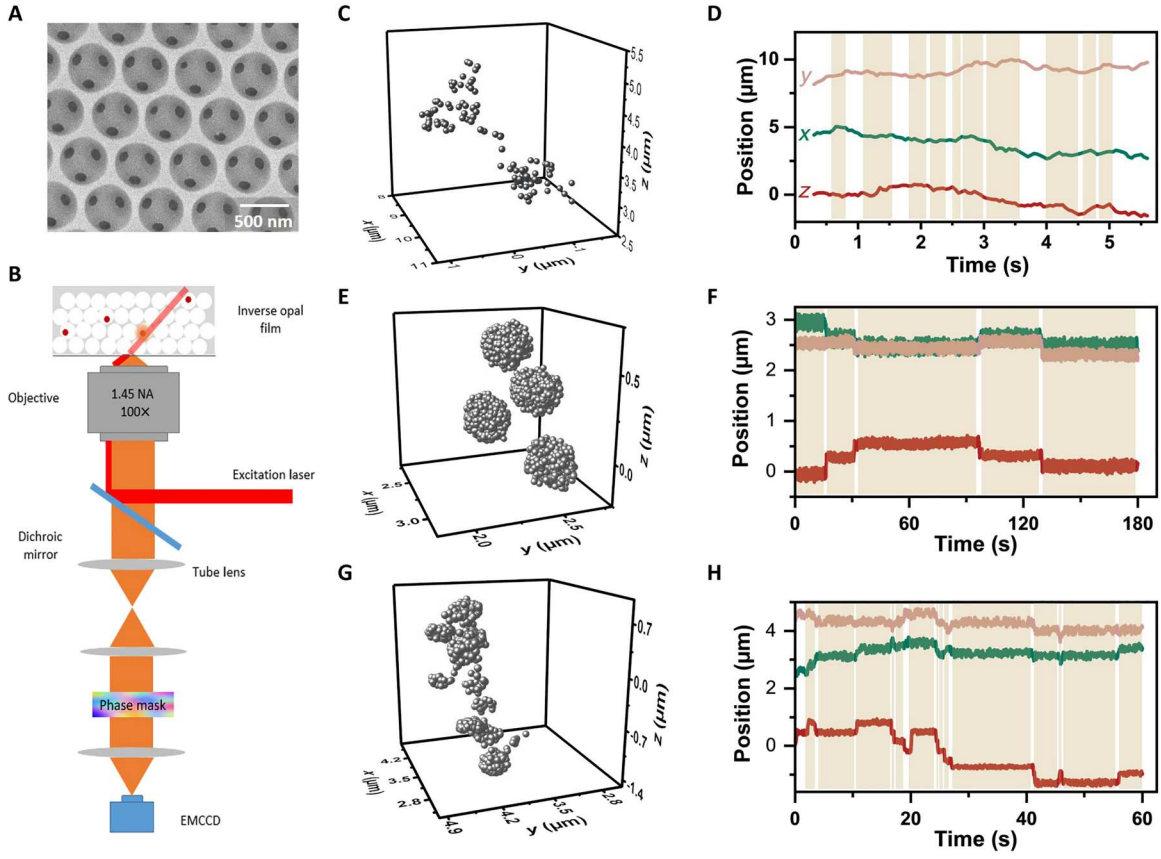

Fig. 1. Experimental schematic and representative trajectories. (**A**) Representative scanning electron microscope image of an inverse opal film structure. (**B**) A microscope was equipped with a phase mask and relay optics that enabled double-helix point spread function imaging. NA, numerical aperture. (**C**) A representative 3D trajectory of a Pt-polystyrene Janus nanomotor with 3% H_2O_2 in an inverse opal. (**D**) Corresponding Cartesian coordinates versus time of a nanomotor in an inverse opal. The highlighted blocks represent time intervals within cavities. (**E**) A representative 3D trajectory of a passive Brownian particle in an inverse opal. (**F**) Corresponding Cartesian coordinates versus time of a passive Brownian particle in an inverse opal. (**G**) A representative 3D trajectory of an activated passive particle in an inverse opal with 3% H_2O_2-fueled nanomotors within the connected pore space. (**H**) Corresponding particle Cartesian coordinates versus time of an activated particle in an inverse opal. Inverse opals used for these three representative trajectories had 500-nm cavities with 136 ± 10–nm–diameter connecting holes.

extended in the strongly confined and interconnected porous void space, perhaps due to the disturbance of the surrounding liquid environment.

Following the early exploration stage at short lag times, Brownian particles in the absence of nanomotors exhibited severely subdiffusive motion, visible in the downward curvature and nearly horizontal slope of the MSD at intermediate lag times (*13*–*15*); this is associated with confining effects within cavities, where particles must search diffusively for holes and also encounter electrostatic barriers to translocation through holes. As shown previously (*37*), at longer lag times (7 to 10 s), Brownian passive particles passed through the transient trapping phase and reestablished an effective diffusive motion at long time scales that was associated with hopping from cavity to cavity. In contrast, nanomotors did not exhibit these severe caging effects due to their unique ability to escape cavities efficiently. Nanomotors found holes rapidly by searching along cavity surfaces and passed through electrostatic barriers easily due to self-propulsion forces (*13*–*15*). For activated passive particles (in the presence of nanomotors), the subdiffusive caging effects were not as marked as for passive particles, and the activated particles also exhibited 4× faster apparent long-time diffusion than passive particles, as shown by the asymptotic behavior of the MSD plots.

In previous work, we demonstrated a direct relationship between the macroscopic long-time diffusion coefficient in a porous medium and a key parameter of microscopic cavity escape kinetics, the so-called sojourn time (t_{soj}) (*14*, *38*) (i.e., the first passage time through a cavity). To determine individual values of t_{soj}, we used a maximum allowed displacement algorithm, analyzing 3D positional fluctuations (Fig. 1, D, F, and H) around a central point (i.e., the cavity center) with a particular characteristic distance (i.e., cavity radius) (*15*). We analyzed complementary cumulative distributions of hundreds of t_{soj} values in inverse opals for nanomotors, passive Brownian particles, and activated Brownian particles (Fig. 2B). The distributions were fitted to a double decaying exponential function $P(t) = A\exp(-t/T_1) + (1 - A)\exp(-t/T_2)$, enabling accurate calculation of the mean sojourn time $\langle t_{soj}\rangle = AT_1 + (1 - A)T_2$. Notably, the $\langle t_{soj}\rangle$ of activated passive particles was reduced significantly, from 9.4 to 4.4 s (compared to passive particles), in the presence of nanomotors powered by 3% H_2O_2. Consistent with previous findings, the $\langle t_{soj}\rangle$ of the nanomotors themselves was reduced by ~20× compared to that of passive particles (*11*). These results

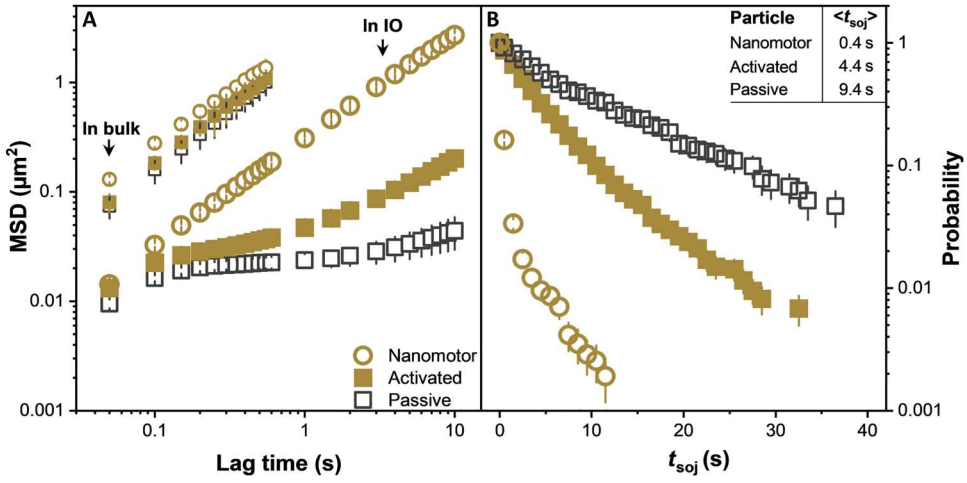

Fig. 2. Statistical analysis of experimental results of nanomotors and passive particles. Nanomotors and passive particles were at a 1:5 ratio in glycerol/water solution (70% by weight). The overall concentration of nanoparticles was approximately 10^{-15} M. (**A**) Mean square displacement of catalytic Janus particle and activated passive particles with 3% H_2O_2 (v/v), as well as passive particles without fuel in bulk solution and in inverse opal films (IO). (**B**) Complementary cumulative probability distributions of cavity sojourn times for different types of nanoparticles.

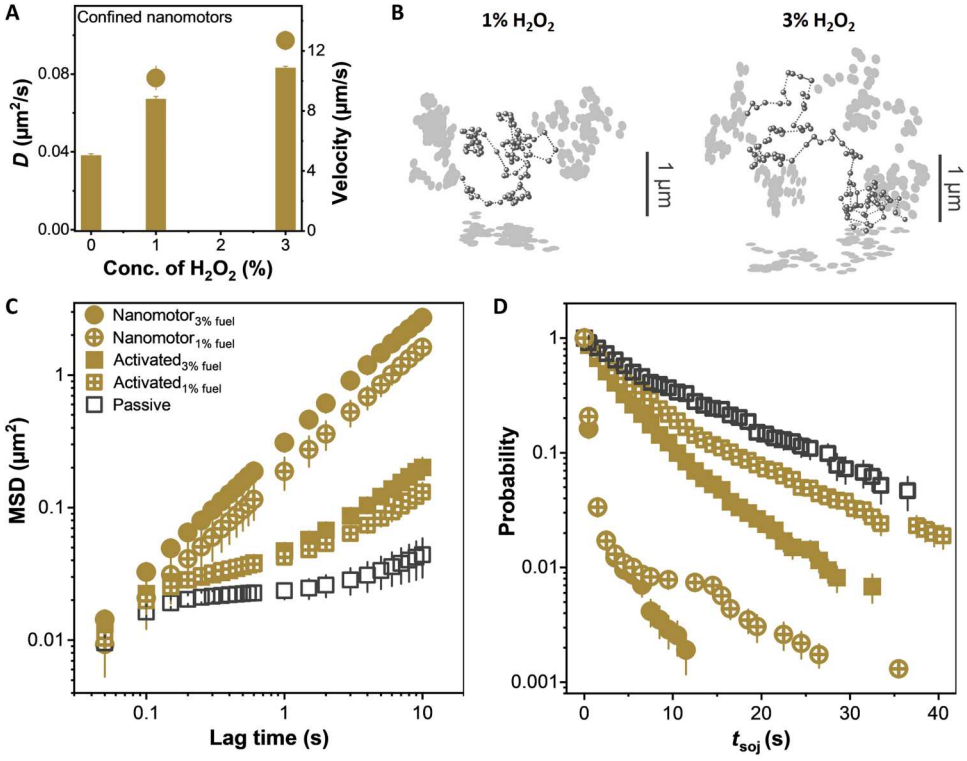

Fig. 3. Observations of nanomotor and activated passive particles in an inverse opal with 1 and 3% H_2O_2 (v/v). Nonfluorescent nanomotors and fluorescent passive nanoparticles were mixed at a 1:5 ratio in glycerol/water solution (70% by weight). (**A**) Diffusion coefficients (columns) and velocities (solid circles) of nanomotors in the inverse opal calculated from short-time diffusion. (**B**) Representative 5-s trajectories of nanomotors activated by 1% (left) and 3% (right) H_2O_2 (v/v). Nanomotors with 3% H_2O_2 explored larger areas in a given time. (**C**) Mean square displacement of catalytic Janus particles, activated passive particles, and passive particles in the inverse opal. (**D**) Complementary cumulative probability distributions of cavity sojourn times for nanoparticles under different conditions. <t_{soj}> values for nanomotors and activated particles with 1% fuel were 0.8 and 7.7 s, respectively.

explicitly indicate that the presence of nanomotors in the interconnected pore space significantly accelerated the cavity escape of Brownian particles, although not to the same degree as the nanomotors themselves.

Considering the very dilute concentrations of passive particles and nanomotors, the activating effect of self-propelled particles apparently produced an unexpected long-distance enhancement of passive particle transport within the interconnected porous void space. In an open system, the strength of far-field hydrodynamic interactions, typically presented as attraction, between identical-sized active and passive particles decays by approximately an order of magnitude over a distance corresponding to twice the particle's diameter (*39*). Thus, the range of this hydrodynamic attraction is generally confined to a spatial extent of 1 to 2 body lengths from the active particles (*27*, *40*). Therefore, as expected, significant enhancement of the motion of passive particles was not observed in the presence of dilute nanomotors in unconfined bulk liquid. It was intriguing to observe that confinement within narrow interconnected pore spaces apparently magnified and extended such hydrodynamic interactions, leading to a substantial enhancement of passive particle motility by nanomotors, even when separated by distance and by the internal interfaces of inverse opals.

Transport enhancement depends on the strength of convection from nanomotors

In general, it is expected that the magnitude of hydrodynamic effects among nanomotors depends on their velocities (*25*). For example, in crowded solutions, fast and slow active particles resulted in different phase segregation of coexisting passive particles (*24*, *25*, *40*, *41*). Therefore, we hypothesized that there would be a correlation between the velocities of nanomotors and confinement-amplified hydrodynamic activation of passive particles. The apparent long-time diffusion of nanomotors is influenced by their swimming speeds. In particular, at times that are long compared to the characteristic rotational diffusion time (τ_R), the apparent diffusion coefficient includes a contribution from thermal Brownian diffusion (D_T) and enhancement from self-propulsion, resulting in $D_{apparent} = D_T + 6\,v^2\tau_R$ in 3D space, where v is the nanomotor velocity (*42*–*44*). Thus, with an increase of fuel concentration from 1 to 3%, the short-time diffusion of confined nanomotors was increased by 25% (Fig. 3A), enlarging the exploration area of nanomotors in a given time (Fig. 3B). As we hypothesized, this enhanced motility of nanomotors was passed on to the activated passive particles within confined pore spaces. Specifically, the increased apparent diffusion (and velocity) of nanomotors resulted in a similar increase in the short-time apparent diffusion of activated passive particles (Fig. 3C). Moreover, the increased motility of nanomotors in the presence of higher fuel concentration resulted in a greater hydrodynamic impact on the cavity escape of passive particles, specifically $<t_{soj}>$ of the passive particles was reduced from 9.4 s for nonactivated particles to 7.7 and 4.4 s in the presence of 1 and 3% H_2O_2-powered nanomotors, respectively (Fig. 3D). This trend provided further support for the conjecture that the enhanced translocation of activated particles originated from confinement-amplified

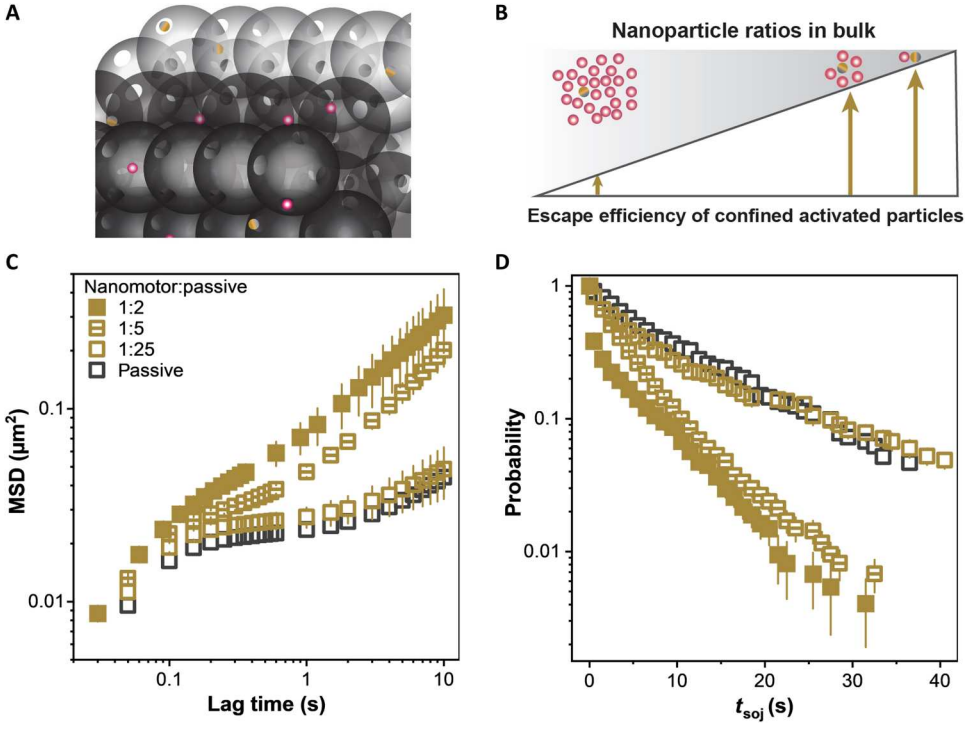

Fig. 4. Influence of nanomotor concentration on the magnitude of activation effect. (**A**) Schematic of a mixture of nanomotors and passive particles in the inverse opal film. The overall concentrations were controlled to be dilute, with much fewer than one particle per cavity. (**B**) Illustration of improved escape efficiency of activated particles with an increasing ratio of nanomotor/passive particle. (**C**) Mean squared displacement (MSD) of activated particles with nanomotor/passive particle ratios of 1:2, 1:5, 1:25, and passive particles only. (**D**) Complementary cumulative probability distributions of cavity sojourn times of activated particles under different conditions. The concentration of activated passive particles was fixed at 10^{-15} M. All particle compositions were dispersed in glycerol/water solution (70%, w/w) with 3% H_2O_2.

hydrodynamic coupling between nanomotors and passive species. Given the velocity dependence of the enhancement, the hydrodynamics may be associated with the flow field generated by nanomotors.

Interparticle distance affects nanomotor-enhanced transport

Hydrodynamic effects depend on the distance between two particles in an open solution. Because of the small size of nanoparticles (40-nm diameter) and dilute concentration (~10^{-15} M), nanomotors did not induce noticeable effects on passive particles in bulk solution (Fig. 2A). However, because the convection generated by self-propulsion is amplified and extended by confinement, its influence on surrounding particles apparently extends to much greater distances. To study the impact of the distance between nanomotors and passive particles on the strength of activation, we varied the concentration of nanomotors with a fixed concentration of passive particles while remaining in the dilute regime overall. Consistent with expectations, a large nanomotor/passive particle ratio induced strong enhancement on the cavity escape of activated particles, resulting in a $<t_{soj}>$ of 2.5 s (Fig. 4). In contrast, activation was gradually reduced with a decreased nanomotor concentration. The cavity escape efficiency of activated passive particles became indistinguishable within experimental error ($<t_{soj}>$ = 9.2 s) from that of passive particles alone when the nanomotor concentration was reduced to a 1:25 active/passive ratio, although the short-time diffusion of the passive particles remained slightly enhanced. Of course, the concentrated regime is more frequently studied and requires large amounts of active particles that may not be accessible for some applications; thus, the novelty of the current results is, in many ways, related to the unexpectedly large effects at low concentrations.

Nanomotors enhance the effective energy of passive particles for hole translocation

Our previous study showed that the enhanced cavity escape of nanomotors relied on efficient surface-mediated searching (*11*), which converted the barrier-limited escape of passive particles to a search-limited process. However, despite the fact that activated passive particles exhibited enhanced cavity escape in the presence of nanomotors, surface-mediated searching was not observed for these passive particles. For example, the distribution of passive particle positions declined sharply near the wall (Fig. 5A), presumably due to electrostatic repulsion, while the distribution of nanomotor positions remained high approaching the cavity wall, consistent with the fact that nanomotors preferentially move along the wall, as reported previously (*45*–*47*).

In addition to the benefits of surface-mediated searching, nanomotors convert external energy into thrust, experiencing a transient velocity spike at pore exits, creating an amplified flow field as demonstrated in simulations (*4*). We hypothesize that this amplified velocity field may also exert an increased hydrodynamic force on vicinal moieties (*48*), including passive particles within the connected pore space. It is intuitively helpful to think of this nanomotor-induced activation as an apparent "effective energy" of passive particles. The enhanced effective energy due to increased advection facilitates the ability of passive particles to overcome energy barriers along streamlines (e.g., translocation between cavities) but is not expected to help passive particles cross streamlines to approach cavity walls that exert strong electrostatic repulsion.

To estimate the enhanced effective energy, we related this metric to an increase in the "effective hole size," an approximation to describe the apparent hole size for a passive particle exiting a cavity in the presence of an electrostatic barrier associated with like-charged walls. In particular, we related an experimentally measured value of $<t_{soj}>$ in the presence of electrostatic repulsion and salt, to an effective hole size determined using a Monte Carlo simulation (*15*). The addition of salt has been shown to screen the electrostatic repulsion between passive particles and cavity walls, thereby enhancing their cavity escape efficiency (*15*, *49*, *50*). For example, the $<t_{soj}>$ of passive particles with 1 mM NaCl was 7.4 s, which was shorter than the value of 9.4 s for passive particles without added salt (Fig. 5B). The cavity escape of activated particles was also enhanced in 1 mM salt solution, for example, $<t_{soj}>$ decreased by 13% from 4.4 to 3.8 s. While it has been reported that salt can decrease the activity of micrometer-scale micromotors (*51*), we did not notice a significant slowing of the much smaller nanomotors (d = 40 nm) under the highly confined conditions of our experiments (fig. S4). The suppression of swimming velocity of micromotors in salt solutions is reported to be sensitive to the surface charges of colloids and dielectric of solvents. Because of the small total charge carried by the individual nanomotors, the confined environment, and the lower permittivity of glycerol/water solution used in our experiments, the suppressing effects of low ionic strength salt solutions were apparently negligible.

Here, we used a Monte Carlo simulation to calculate the effective hole sizes associated with various sojourn times and specifically determined the effective hole sizes for the sojourn times of activated (d = 90 nm) and passive particles (d = 77 nm) in the presence of 1 mM salt (Fig. 5C). This means, for example, that the mean sojourn time of a negatively charged passive particle through a negatively charged hole with a physical diameter of 136 nm corresponds to the escape of the same size uncharged particle through a 77-nm uncharged hole. According to Derjagin-Landau-Verwey-Overbeek (DLVO) theory, the superposition of electrostatic repulsion and van der Waals attraction defines the interactions between a charged particle and a like charged surface. To specifically estimate the enhancement of the effective energy due to activation, the form of the DLVO potential was visualized in the context of the effective hole sizes (see the Supplementary Materials for details). The dimensionless potential energy (normalized by the thermal energy k_BT) for a 40-nm nanoparticle at the entrance of 136-nm hole is shown in Fig. 5D. As indicated on the figure, a particle with thermal energy of k_BT has sufficient energy to pass through a hole with an effective width of 72 nm. Because activated particles do not move across the streamline, the widened apparent effective hole size, 90 nm, was contributed by enhanced effective energy (ΔE), which was approximated as 0.8 k_BT in the presence of dilute nanomotors.

DISCUSSION

We speculate that the long-range hydrodynamic coupling described above may lead to interactions that boost the effective energy of passive particles, thereby facilitating efficient translocation in porous media. Previous work has demonstrated that phoretic flow can transmit attractive hydrodynamic drag forces to surrounding particles in bulk solution (*48*, *52*). Because confinement apparently

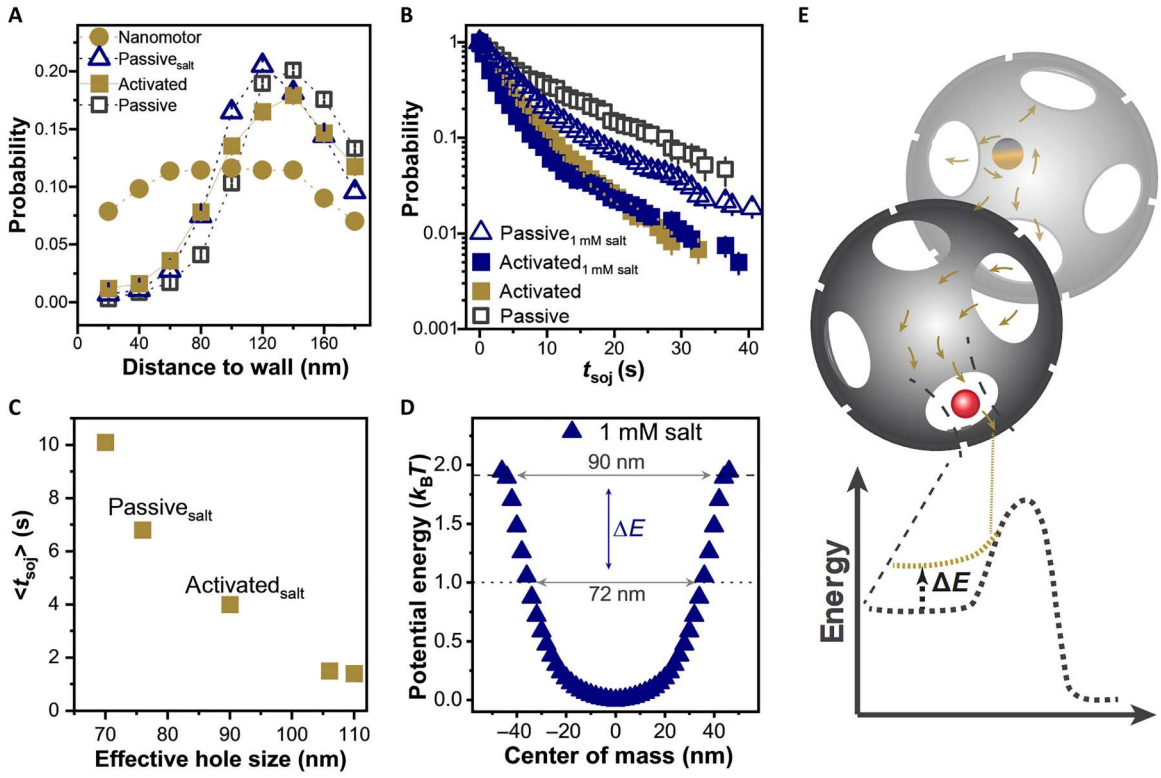

Fig. 5. Effective energy boost for hole translocation of passive particles. (**A**) Distribution of wall-particle distances of 40-nm-diameter nanoparticles inside one spherical cavity (d = 500 nm). (**B**) Distribution of cavity sojourn times of activated and passive particles in different solutions. (**C**) Dependency of effective pore sizes and <t_{soj}> from Monte Carlo simulations. (**D**) Dimensionless potential energy of a negatively charged nanoparticle in the entrance plane of a negatively charged hole with a diameter of 136 nm connecting to a cavity 500 nm in diameter. The horizontal axis represents the lateral position of the center of the nanoparticle. (**E**) Schematic illustrating that adjacent nanomotors enhance the effective energy of passive particles in a separated cavity, assisting in overcoming the energy barrier along streamlines.

amplifies and extends the hydrodynamic effects of nanomotors in porous void spaces, long-range hydrodynamic effects may enhance the apparent effective energy of coexisting passive Brownian particles that are separated by interfaces and distance, helping them to overcome energy barriers associated with cavity escape along streamlines. Further theoretical studies are required to fully understand the details of the magnified hydrodynamic interactions of nanomotors with passive species in confined environments. While the transport efficiency of activated passive particles continued to increase over the range of concentrations studied (up to a 1:2 active/passive ratio), we anticipate that more complicated behavior would eventually be observed at very high nanomotor concentrations due to short-range interactions (steric effects, collisions, and electrostatic and hydrodynamic interactions). It is expected that the enhancement of transport will require careful tuning of nanomotor concentration to adjust long- and short-range interactions associated with particle-particle distances. Overall, confinement-amplified effects can enhance the apparent effective energy significantly for passive species to translocate through pore constrictions, and the magnitude of the apparent energy boost can be tuned by the activity and concentration of nanomotors.

Self-propelled nanoparticles exhibit unique swimming and transport behaviors, and their hydrodynamic effects are known to influence surrounding passive species within short distances on the order of the particle size. Here, we studied the impacts of dilute well-separated nanomotors on passive nanoparticles in an interface-confined environment. In contrast to the negligible coupling effects observed in unconfined solutions with dilute nanoparticles, the convection caused by nanomotors in interconnected narrow pore spaces was magnified and extended, activating passive Brownian particles and enhancing their short-time diffusion and cavity escape efficiency despite the fact that the nanomotors and passive nanoparticles were separated by interfaces and distances that are much larger than the particle sizes. The long-range of the nanomotors′ impact indicated that confined environments can amplify hydrodynamic effects of self-propulsion. Moreover, the magnitude of this influence was related to the activity and concentration of the nanomotors.

Because activated passive particles were repelled by the cavity surface, in contrast to the trajectories of nanomotors themselves, the activation by nanomotors did not change the intrinsic searching mechanism of passive particles. In particular, the activated passive particles pursued a 3D search for exit holes throughout the cavity volume, in contrast with self-propelled nanomotors, which search along cavity walls. However, by comparing trajectories and computational simulations, we found that the presence of nanomotors enhanced the effective energy of confined passive species for translocation. For example, in one particular experimental realization, we found an apparent 0.8-k_BT increase of the effective energy of passive particles. Our current results suggest that nanomotors

have the potential to mobilize passive particles in confined pore spaces or even break down aggregates of passive moieties in complex media, such as membranes. This intriguing result suggests that a small amount of nanomotors can have important impacts in complex environments and may provide a general strategy for transport enhancement in complex environments.

MATERIALS AND METHODS

Experimental design

Synthesis of inverse opal

Monodispersed polystyrene particles (500-nm diameter) were purchased from MilliporeSigma (MA) and used as received. A 10% (w/w) stock particle suspension (0.25 ml) was diluted by adding 9.75 ml of high-performance liquid chromatography–grade water (≥99.9%; Thermo Fisher Scientific, MA) followed by 20-min sonication. Meanwhile, 1 ml of tetraethyl orthosilicate (TEOS; Sigma-Aldrich, MA) solution was mixed with 1.5 ml of anhydrous ethanol (Decon Laboratories Inc., PA) and hydrolyzed by 1 ml of 0.1 M HCl (Thermo Fisher Scientific, MA), and the hydrolyzation process required approximately 1 hour under vigorous stirring. Then, 90 or 110 μl of hydrolyzed TEOS solution was added to the diluted particle solution, keeping the TEOS concentration in the range of 10^{-15} mM. A 25-mm-diameter microscope glass slide was used as a substrate, and it was vertically suspended in a beaker containing the colloidal beads and standard TEOS solution. The solution was evaporated in a 65°C oven for 48 hours to form a thin film of opal structure on the glass slide. The resulting inverse opal film was then pyrolyzed in a furnace at 450°C for 2 hours to remove the templating polystyrene particles and to form a solid silica inverse opal film.

Synthesis of nanomotors

Nanomotors with diameter of 40 nm were prepared from fluorophore-labeled polystyrene nanoparticles (Invitrogen, MA). The aqueous nanoparticle solution (w/w = 2.5%) as purchased was 10× diluted by ethanol and then spin-coated on 18 cm–by–18 cm slides to form nanoparticle submonolayers. The immobilized particles were sputter coated with a ~1-nm layer of Pt on the exposed particle hemisphere. The coating was performed using a Cressington 108 Auto sputter coater, with a pure Pt sputter target (57-mm diameter; purity, 99.95%; Ted Pella). The metal layer thickness for each sample was monitored via a Cressington Thickness Monitor. After metal deposition, the particles were liberated from the glass slide to water by sonication (90 s per slide).

Confined nanoparticles in the inverse opal film

Nanomotors and passive particles were mixed in certain ratios (1:5, 1:2, or 1:25) in bulk glycerol/water solutions. Then, 400 μl of a mixed nanoparticle solution was added onto the silica inverse opal film grown on a glass slide and incubated for 24 hours. To power the nanomotors, H_2O_2 solution was slowly added to the inverse opal film to avoid bubbles. Imaging was carried out 1 min later after the addition of H_2O_2.

Supplementary Materials

This PDF file includes:

Supplementary Text
Figs. S1 to S5
References

REFERENCES AND NOTES

1. L. Soler, V. Magdanz, V. M. Fomin, S. Sanchez, O. G. Schmidt, Self-propelled micromotors for cleaning polluted water. *ACS Nano* **7**, 9611–9620 (2013).
2. C. Wang, B. E. Fernández de Ávila, R. Mundaca-Uribe, M. A. Lopez-Ramirez, D. E. Ramírez-Herrera, S. Shukla, N. F. Steinmetz, J. Wang, Active delivery of VLPs promotes anti-tumor activity in a mouse ovarian tumor model. *Small* **16**, e1907150 (2020).
3. C. P. Thome, W. S. Hoertdoerfer, J. R. Bendorf, J. G. Lee, C. W. I. Shields, Electrokinetic active particles for motion-based biomolecule detection. *Nano Lett.* **23**, 2379–2387 (2023).
4. F. Yang, S. Qian, Y. Zhao, R. Qiao, Self-diffusiophoresis of janus catalytic micromotors in confined geometries. *Langmuir* **32**, 5580–5592 (2016).
5. C, Bechinger, R. Di Leonardo, H. Löwen, C. Reichhardt, G. Volpe, G. Volpe, Active particles in complex and crowded environments. *Rev. Mod. Phys.* **88**, 045006 (2016).
6. G. Volpe, I. Buttinoni, D. Vogt, H. J. Kümmerer, C. Bechinger, Microswimmers in patterned environments. *Soft Matter* **7**, 8810–8815 (2011).
7. J. Simmchen, J. Katuri, W. E. Uspal, M. N. Popescu, M. Tasinkevych, S. Sánchez, Topographical pathways guide chemical microswimmers. *Nat. Commun.* **7**, 10598 (2016).
8. S. Das, A. Garg, A. I. Campbell, J. Howse, A. Sen, D. Velegol, R. Golestanian, S. J. Ebbens, Boundaries can steer active Janus spheres. *Nat. Commun.* **6**, 8999 (2015).
9. H. R. Jiang, N. Yoshinaga, M. Sano, Active motion of a Janus particle by self-thermophoresis in a defocused laser beam. *Phys. Rev. Lett.* **105**, 268302 (2010).
10. T. Bhattacharjee, S. S. Datta, Bacterial hopping and trapping in porous media. *Nat. Commun.* **10**, 2075 (2019).
11. H. Wu, B. Greydanus, D. K. Schwartz, Mechanisms of transport enhancement for Self-propelled nanoswimmers in a porous matrix. *Proc. Natl. Acad. Sci. U.S.A.* **118**, e2101807118 (2021).
12. P. de Anna, A. A. Pahlavan, Y. Yawata, R. Stocker, R. Juanes, Chemotaxis under flow disorder shapes microbial dispersion in porous media. *Nat. Phys.* **17**, 68–73 (2021).
13. D. Wang, H. Wu, L. Liu, J. Chen, D. K. Schwartz, Diffusive escape of a nanoparticle from a porous cavity. *Phys. Rev. Lett.* **123**, 118002 (2019).
14. H. Wu, D. K. Schwartz, Nanoparticle tracking to probe transport in porous media. *Acc. Chem. Res.* **53**, 2130–2139 (2020).
15. H. Wu, R. Sarfati, D. Wang, D. K. Schwartz, Electrostatic barriers to nanoparticle accessibility of a porous matrix. *J. Am. Chem. Soc.* **142**, 4696–4704 (2020).
16. J. G. Lee, R. R. Raj, C. P. Thome, N. B. Day, P. Martinez, N. Bottenus, A. Gupta, C. W. I. Shields, Bubble-based microrobots with rapid circular motions for epithelial pinning and drug delivery. *Small* **19**, e2300409 (2023).
17. F. Zhang, J. Zhuang, Z. Li, H. Gong, B. E. F. de Ávila, Y. Duan, Q. Zhang, J. Zhou, L. Yin, E. Karshalev, W. Gao, V. Nizet, R. H. Fang, L. Zhang, J. Wang, Nanoparticle-modified microrobots for in Vivo antibiotic delivery to treat acute bacterial pneumonia. *Nat. Mater.* **21**, 1324–1332 (2022).
18. J. R. Baylis, J. H. Yeon, M. H. Thomson, A. Kazerooni, X. Wang, A. E. St. John, E. B. Lim, D. Chien, A. Lee, J. Q. Zhang, J. M. Piret, L. S. Machan, T. F. Burke, N. J. White, C. J. Kastrup, Self-propelled particles that transport cargo through flowing blood and halt hemorrhage. *Sci. Adv.* **1**, e1500379 (2015).
19. A. A. Solovev, S. Sanchez, O. G. Schmidt, Collective Behaviour of Self-Propelled Catalytic Micromotors. *Nanoscale* **5**, 1284–1293 (2013).
20. K. V. Nguyen, S. D. Minteer, DNA-functionalized Pt nanoparticles as catalysts for chemically powered micromotors: Toward signal-on motion-based DNA biosensor. *Chem. Commun. (Camb).* **51**, 4782–4784 (2015).
21. J. Tong, D. Wang, D. Wang, F. Xu, R. Duan, D. Zhang, J. Fan, B. Dong, Visible-light-driven water-fueled ecofriendly micromotors based on iron phthalocyanine for highly efficient organic pollutant degradation. *Langmuir* **36**, 6930–6937 (2020).
22. Y. Ren, H. Li, J. Liu, M. Zhou, J. Pan, Crescent-shaped micromotor sorbents with sulfonic acid functionalized convex surface: The synthesis by a Janus emulsion strategy and adsorption for Li+. *J. Hazard. Mater.* **422**, 126870 (2022).
23. K. M. Yamada, M. Sixt, Mechanisms of 3D cell migration. *Nat. Rev. Mol. Cell Biol.* **20**, 738–752 (2019).
24. F. Kümmel, P. Shabestari, C. Lozano, G. Volpe, C. Bechinger, Formation, compression and surface melting of colloidal clusters by active particles. *Soft Matter* **11**, 6187–6191 (2015).
25. T. Kolb, D. Klotsa, Active binary mixtures of fast and slow hard spheres. *Soft Matter* **16**, 1967–1978 (2020).
26. W. Gao, A. Pei, X. Feng, C. Hennessy, J. Wang, Organized self-assembly of Janus micromotors with hydrophobic hemispheres. *J. Am. Chem. Soc.* **135**, 998–1001 (2013).
27. W. Wang, W. Duan, A. Sen, T. E. Mallouk, Catalytically powered dynamic assembly of rod-shaped nanomotors and passive tracer particles. *Proc. Natl. Acad. Sci.* **110** (44), 17744–17749 (2013).

28. E. B. van der Wee, B. C. Blackwell, F. Balboa Usabiaga, A. Sokolov, I. T. Katz, B. Delmotte, M. M. Driscoll, A simple catch: Fluctuations enable hydrodynamic trapping of microrollers by obstacles. *Sci. Adv.* **9**, eade0320 (2023).
29. B. Liebchen, A. K. Mukhopadhyay, Interactions in active colloids. *J. Phys. Condens. Matter* **34**, 083002 (2022).
30. S. Williams, R. Jeanneret, I. Tuval, M. Polin, Confinement-induced accumulation and demixing of microscopic active-passive mixtures. *Nat. Commun.* **13**, 4776 (2022).
31. X. L. Wu, A. Libchaber, Particle diffusion in a quasi-two-dimensional bacterial bath. *Phys. Rev. Lett.* **84**, 3017–3020 (2000).
32. S. C. Takatori, J. F. Brady, A theory for the phase behavior of mixtures of active particles. *Soft Matter* **11**, 7920–7931 (2015).
33. B. Hatton, L. Mishchenko, S. Davis, K. H. Sandhage, J. Aizenberg, Assembly of large-area, highly ordered, crack-free inverse opal films. *Proc. Natl. Acad. Sci.* **107**, 10354–10359 (2010).
34. D. Wang, A. Agrawal, R. Piestun, D. K. Schwartz, Enhanced information content for three-dimensional localization and tracking using the double-helix point spread function with variable-angle illumination epifluorescence microscopy. *Appl. Phys. Lett.* **110**, 211107 (2017).
35. S. L. Dettmer, S. Pagliara, K. Misiunas, U. F. Keyser, Anisotropic diffusion of spherical particles in closely confining microchannels. *Phys Rev E Stat Nonlin Soft Matter Phys.* **89**, 062305 (2014).
36. X. Yang, C. Liu, Y. Li, F. Marchesoni, P. Hänggi, H. P. Zhang, Hydrodynamic and entropic effects on colloidal diffusion in corrugated channels. *Proc. Natl. Acad. Sci.* **114**, 9564–9569 (2017).
37. H. Wu, D. Wang, D. K. Schwartz, Connecting hindered transport in porous media across length scales: From single-pore to macroscopic. *J. Phys. Chem. Lett.* **11**, 8825–8831 (2020).
38. D. Wang, D. K. Schwartz, Non-brownian interfacial diffusion: Flying, hopping, and crawling. *J. Phys. Chem. C* **124**, 19880–19891 (2020).
39. T. Ishikawa, M. P. Simmonds, T. J. Pedley, Hydrodynamic interaction of two swimming model micro-organisms. *J. Fluid Mech.* **568**, 119–160 (2006).
40. P. Dolai, A. Simha, S. Mishra, Phase separation in binary mixtures of active and passive particles. *Soft Matter* **14**, 6137–6145 (2018).
41. J. Stenhammar, R. Wittkowski, D. Marenduzzo, M. E. Cates, Activity-induced phase separation and self-assembly in mixtures of active and passive particles. *Phys. Rev. Lett.* **114**, 018301 (2015).
42. J. R. Howse, R. A. L. Jones, A. J. Ryan, T. Gough, R. Vafabakhsh, R. Golestanian, Self-motile colloidal particles: From directed propulsion to random walk. *Phys. Rev. Lett.* **99**, 048102 (2007).
43. B. Greydanus, M. Saleheen, H. Wu, A. Heyden, J. W. Medlin, D. K. Schwartz, Probing surface-adsorbate interactions through active particle dynamics. *J. Colloid Interface Sci.* **614**, 425–435 (2022).
44. B. Greydanus, J. W. Medlin, D. K. Schwartz, Elucidating the influence of metal surface composition on organic adsorbate binding using active particle dynamics. *J. Phys. Chem. C* **127**, 1006–1014 (2023).
45. A. Mozaffari, N. Sharifi-Mood, J. Koplik, C. Maldarelli, Self-diffusiophoretic colloidal propulsion near a solid boundary. *Phys. Fluids* **28**, 053107 (2016).
46. W. E. Uspal, M. N. Popescu, S. Dietrich, M. Tasinkevych, Self-propulsion of a catalytically active particle near a planar wall: From reflection to sliding and hovering. *Soft Matter* **11**, 434–438 (2015).
47. S. Das, Z. Jalilvand, M. N. Popescu, W. E. Uspal, S. Dietrich, I. Kretzschmar, Floor- or ceiling-sliding for chemically active, gyrotactic, sedimenting Janus particles. *Langmuir* **36**, 7133–7147 (2020).
48. Y. Cheng, F. Mou, M. Yang, S. Liu, L. Xu, M. Luo, J. Guan, Long-range hydrodynamic communication among synthetic self-propelled micromotors. *Cell Rep. Phys. Sci.* **3**, 100739 (2022).
49. S. G. Kluijtmans, E. H. A. de Hoog, A. P. Philipse, Self-diffusion of charged colloidal tracer spheres in transparent porous glass media: Effect of ionic strength and pore size. *J. Chem. Phys.* **108**, 7469–7477 (1998).
50. T. Stylianopoulos, M. Z. Poh, N. Insin, M. G. Bawendi, D. Fukumura, L. L. Munn, R. K. Jain, Diffusion of particles in the extracellular matrix: The effect of repulsive electrostatic interactions. *Biophys. J.* **99**, 1342–1349 (2010).
51. A. Brown, W. Poon, Ionic effects in self-propelled pt-coated Janus swimmers. *Soft Matter* **10**, 4016–4027 (2014).
52. E. E. Michaelides, Brownian movement and thermophoresis of nanoparticles in liquids. *Int. J. Heat Mass Transf.* **81**, 179–187 (2015).
53. W. R. Bowen, A. N. Filippov, A. O. Sharif, V. M. Starov, A model of the interaction between a charged particle and a pore in a charged membrane surface. *Adv. Colloid Interface Sci.* **81**, 35–72 (1999).
54. G. Volpe, S. Gigan, G. Volpe, Simulation of the active Brownian motion of a microswimmer. *Am. J. Phys.* **82**, 659–664 (2014).

Acknowledgments

Funding: This work was supported by the U.S. Department of Energy, Office of Science, Basic Energy Sciences, under Award No. DE-SC0001854. **Author contributions:** Conceptualization: D.K.S. Methodology: A.S., H.W., and D.K.S. Investigation: A.S. Visualization: A.S. Supervision: D.K.S. Writing—original draft: A.S. Writing—review and editing: A.S., D.K.S., and H.W. **Competing interests:** The authors declare that they have no competing interests. **Data and materials availability:** All data and code needed to evaluate the conclusions in the paper are present in the paper and/or the Supplementary Materials and on zenodo.org/record/8352480.

Submitted 16 June 2023
Accepted 2 November 2023
Published 1 December 2023
10.1126/sciadv.adj2208